Validation of decomposition models for solar irradiance at high latitudes: A preliminary study

Validation of decomposition models for solar irradiance at high latitudes: A preliminary study

M Manni[1], A Nocente[2], K Skeie[2], M Bellmann[2], G Lobaccaro[1]

[1] Department of Civil and Environmental Engineering, Norwegian University of Science and Technology, Trondheim, Norway
[2] SINTEF AS, Trondheim, Norway

Corresponding author's email: mattia.manni@ntnu.no

Abstract. The accurate estimation of buildings' solar potential contributes to boost the exploitation of solar energy at high latitudes. The decomposition of global irradiation into the direct and diffuse fractions is a fundamental step of the solar irradiance model chain. Diffuse and direct irradiation are, in fact, rarely measured. Previous works recommended Yang4 as the decomposition model with the best overall performance. However, in geographically limited applications, quasi-universal decomposition models such as Yang4 and Engerer4 can be outperformed by local models (i.e., models parametrized with climate-specific data) such as Skartveit3 and Starke3. This makes necessary to perform local validation studies to verify the findings from worldwide validation studies. In this study, the four decomposition models are implemented in Python and experimentally validated against one-minute solar irradiance data (i.e., direct and diffuse irradiance) of Trondheim (Lat. 63°26' N, Norway). Two months representative of clear sky (August) and overcast (October) conditions are considered. The study confirms that the Yang4 model performed the best for high-latitude application: the nMBE ranged from -0.54% (August) to 0.65% (October), the nRMSE from 17.18% (August) to 22.29% (October), and the R^2 from 0.96 (August) to 0.97 (October). However, Skartveit3 combines a level of performance close to Yang4 with the lower number of input parameters.

1. Introduction

Installed solar power capacity in Norway has grown from 15 MW in 2015 to 225 MW in 2021 [1]. This growth happened later than other countries in Europe, and this is mostly related to the belief that the Nordic countries has low solar energy potential compared to Continental Europe [2]. However, the distribution of solar radiation throughout the year in the Nordic countries is different from the Continental Europe, with less daylight hours in wintertime and greater sunlight availability in summertime [3,4], but not necessarily lower. Within this framework, accurate estimation of solar potential of buildings contributes to boost the exploitation of solar energy at high latitudes. To quantify the solar irradiation impinging on a surface, the amount of direct normal irradiance (DNI) and diffuse horizontal irradiance (DHI) needs to be known. However, on-site ground measurements of DNI and DHI are not common. These quantities are usually estimated from global horizontal irradiance (GHI) using empirical decomposition models. Although the decomposition models have been improved and developed in last decades, these continue to be influenced by the selected location, as they are parametrized with site-specific data [5,6]. Therefore, local models (i.e., models parametrized with climate data from a restricted geographic area) can outperform models presented as quasi-universal when applied to the location where the data originates [7].

Previous works recommended Yang4 as the quasi-universal decomposition model with the best overall performance. In this study, this model is experimentally validated and compared with alternatives models such as the Engerer4 (quasi-universal), the Starke3 and the Skartveit3 (both climate-specific) models, using solar irradiation data collected in Trondheim (Lat. 63° 26' 48.5772" N, Norway). The research goal is to determine which decomposition model performs best locally (i.e., restricted geographic area) at high latitudes. The novelty of the study is represented by the application of a comparative validation workflow at high latitudes. Moreover, this work contributes to boost the transition from the currently used two-dimensional solar maps [8,9], where the visualization of solar potential is limited to the rooftop surfaces, to the three-dimensional solar cadastres, where buildings' façades are also assessed [10,11].

2. Method and materials

2.1. Workflow

The workflow implemented in this study is divided into four stages: (stage *i*) data acquisition, (stage *ii*) data quality check, (stage *iii*) solar decomposition, and (stage *iv*) experimental validation (Figure 1). In the stage *i*, data regarding solar irradiation is acquired from a sun tracker located in the Sentralbygg 1 at NTNU and the Solar Radiation service from Copernicus Atmosphere Monitoring Service (CAMS). Furthermore, the location of the case study (e.g., latitude, longitude), and the analyzed time interval (e.g., start date and end date) are defined. A Python script is implemented to retrieve the datasets from the respective databases and combine them into a new data-frame.

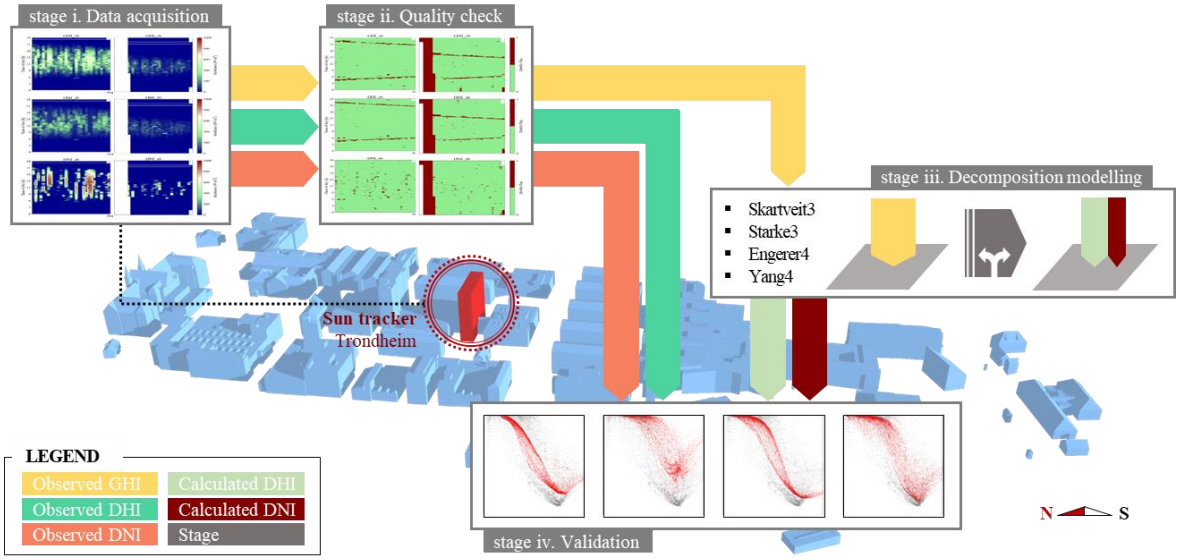

Figure 1. Overview of the workflow followed in this study. The four stages (e.g., data acquisition, data quality check, decomposition modelling, and validation) are highlighted together with the solar irradiance dataflows. On the background, a tri-dimensional view of the Gløshaugen campus.

In the stage *ii*, the data recorded by the sun tracker is classified according to the quality check scheme described in section 2.4. A Python script is implemented to assign a quality flag (QF) to each datapoint which is then used to filter out the erroneous measurements from the validation process.

The decomposition modelling is included in stage *iii*, and it is applied to the solar irradiation dataset acquired during the stage *i*. The GHI is split into the DHI and the DNI.

During stage *iv*, the solar irradiation outputs from the previous stage are used to estimate the clearness index (k_t) and the diffuse fraction (k_d). The calculated k_d is validated against the observed k_d. Three statistical indicators are used to evaluate the accuracy of the results: the Normalized Mean Bias Error (nMBE), the Normalized Root Mean Square Error (nRMSE), and the coefficient of determination (R^2).

2.2. Decomposition models

2.2.1. Skartveit3. The Skartveit3 model is a decomposition model parametrized with solar irradiance data from Bergen [12]. Although the model was implemented for hourly data, in this study, it is applied to one-minute data of solar irradiation. The k_d estimated by the Skartveit3 model is calculated as:

$$k_d^{SKARTVEIT3} = \begin{cases} 1, k_t \leq 0.22 \\ 1-(1-d_1)\cdot\left(0.11\cdot\sqrt{K}+0.15\cdot K+0.74\cdot K^2\right), 0.22 < k_t \leq k_2 \\ d_2\cdot k_2\cdot\dfrac{1-k_t}{k_t\cdot(1-k_2)}, k_2 < k_t \leq k_{max} \\ 1-\dfrac{k_{max}\cdot(1-d_{max})}{k_t}, k_t > k_{max} \end{cases} \quad (1)$$

Where Z is the solar elevation in degrees and the other coefficients are defined as described in [12].

Furthermore, the term $\Delta(k_t, Z, \sigma_3)$ is added to $k_d^{SKARTVEIT3}$ to take into account the effect of variable or inhomogeneous clouds, when σ_3 is greater than zero. The σ_3 is the hourly variability index defined as the root mean squared deviation between the clear sky index of the hour in question (ρ) and, respectively, the preceding (ρ_{-1}) and the following (ρ_{+1}) hour [12].

$$\Delta(k_t, Z, \sigma_3) = \begin{cases} -3\cdot k_L^2\cdot(1-k_L)\cdot\sigma_3^{1.3}, 0.14 \leq k_t < k_x \\ 3\cdot k_R\cdot(1-k_R)^2\cdot\sigma_3^{0.6}, k_x \leq k_t \leq k_x+0.71 \\ 0, k_t > k_x+0.71 \end{cases} \quad (2)$$

2.2.2. Starke3. The Starke3 model is an example of climate-specific models. Its coefficients were determined by fitting local data. The set of coefficients identified for the continental sub-artic climate (Dfc) climate zone (i.e., the climate zone of Trondheim according to Köppen Geiger classification [15]) is used in this study [7]. To calculate the k_d, the equation (3) is used when κ is greater than 1.05 and k_t is higher than 0.75. Otherwise, Equation (4) is followed.

$$\boldsymbol{k_d^{STARKE3}} = \frac{\mathbf{1}}{\mathbf{1}+\boldsymbol{e^{\beta_0+\beta_1\cdot k_t+\beta_2\cdot AST+\beta_3\cdot\alpha+\beta_4\cdot k_{t,daily}+\beta_5\cdot\psi+\beta_6\cdot G_{csky}+\beta_7\cdot k_{t,hourly}}}} \quad (3)$$

$$k_d^{STARKE3} = \frac{1}{1+e^{\beta_8+\beta_9\cdot k_t+\beta_{10}\cdot AST+\beta_{11}\cdot\alpha+\beta_{12}\cdot k_{t,daily}+\beta_{13}\cdot\psi+\beta_{14}\cdot G_{csky}+\beta_{15}\cdot k_{t,hourly}}} \quad (4)$$

2.2.3. Engerer4. The Engerer4 model is a quasi-universal model which has been implemented by Bright and Engerer [13] who updated the Engerer2 [14]model by recalculating the parameters with datasets from 75 different stations worldwide. It is the most recent model from Engerer and it calculates the k_d accordingly to the equation:

$$k_d^{ENGERER4} = C + \frac{1-\mathrm{C}}{1+e^{\beta_0+\beta_1\cdot k_t+\beta_2\cdot AST+\beta_3\cdot\mathrm{Z}+\beta_4\cdot\Delta k_{tc}}} + \beta_5\cdot k_{de} \quad (5)$$

where AST is the apparent solar time, Z is the zenith angle, and Δk_{tc} is the deviation between k_{tc} and k_t. The C and the β-coefficients are the same presented in [13]. Finally, the k_{de} is calculated as:

$$k_{de} = \max\left(0, 1-\frac{G_{csky}}{G_h}\right) \quad (6)$$

2.2.4. Yang4. Introduced in [15] as an application of temporal-resolution cascade, the Yang4 model was able to replace Engerer2 as the new quasi-universal model. The model consists of an enhanced version of Yang2 model where the satellite-based k_d is replaced by the hourly k_d estimated by the Engerer2 model. This improvement enables the real-time application of the Yang4. The k_d is determined accordingly to the equation:

$$k_d^{YANG4} = C + \frac{1-\mathrm{C}}{1+e^{\beta_0+\beta_1\cdot k_t+\beta_2\cdot AST+\beta_3\cdot\mathrm{Z}+\beta_4\cdot\Delta k_{tc}+\beta_4\cdot k_{d,hourly}^{ENGERER2}}} + \beta_5\cdot k_{de} \quad (7)$$

2.3. Solar radiation dataset

Solar irradiance data used in this work refer to Trondheim. By being located along the Trondheimsfjord at the coastal line, Trondheim is representative for many other settlements with similar climatic conditions that are characterized by high reflection from the sea and significant moister content in the air. The solar irradiance data is acquired from the SOLYS2 sun tracker (Kipp & Zonen) installed in the Sentralbygg 1 of NTNU Gløshaugen Campus. The dataset includes GHI, DHI, and DNI, with a time resolution of one minute. October 2021 and August 2022 are selected to validate the models which are, on the annual basis, the most representative months with both clear sky and overcast sky conditions.

In addition, other solar radiation parameters are retrieved from CAMS to be used as model predictors. In fact, the GHI extra atmosphere (GHI_{extra}) and the clear sky GHI (GHI_{csky}) are estimated for the same months, with one-minute time resolution.

2.4. Data quality check

Although there is a lack of universally recognized processes for data quality control when it comes to solar irradiance [7,16,17], the one proposed by Long and Shi [18], and more recently used by the Baseline Surface Radiation Network (BSRN), is the most popular among scholars and experts in this field. In the hereby presented study, this protocol is applied to classify each datapoint, and then to exclude data which shows a low level of accuracy. To filter out the erroneous measurements, the data acquired by the sun tracker are compared to both the global physically possible limits and the extremely rare limits (Table 1) determined according to Long and Shi [18]. In addition, other two tests (Table 1) are performed to detect erroneous measurements from equipment. The deviation of the observed GHI from the sum of the direct horizontal irradiance (BHI) and the DHI is assessed together with the diffuse ratio (k_d). However, when measured or calculated GHI is less than 50W/m^2 or Z is minor than 93°, these tests are not possible since the sensors show a lower accuracy when the sun is very low on the horizon and the solar radiation amounts are minimal.

Table 1. Data quality check scheme applied to the data collected by the sun tracker in Trondheim (Norway).

Variable	Lower limit	Upper limit
	Physical limits	
GHI	$-4\,W/m^2$	$1.5 \cdot E_{0n} \cdot \cos^{1.2} Z + 100\,W/m^2$
DHI	$-4\,W/m^2$	$0.95 \cdot E_{0n} \cdot \cos^{1.2} Z + 50\,W/m^2$
DNI	$-4\,W/m^2$	E_{0n}
	Extremely rare limits	
GHI	$-2\,W/m^2$	$1.2 \cdot E_{0n} \cdot \cos^{1.2} Z + 50\,W/m^2$
DHI	$-2\,W/m^2$	$0.75 \cdot E_{0n} \cdot \cos^{1.2} Z + 30\,W/m^2$
DNI	$-2\,W/m^2$	$0.95 \cdot E_{0n} \cdot \cos^{0.2} Z + 10\,W/m^2$
	Closure comparison	
$\left\lvert\frac{GHI}{DHI + BHI}\right\rvert$	N/A	$1.08\ if\ Z \leq 75°$ and $\mathrm{DHI} + \mathrm{BHI} > 50\,W/m^2$ $1.15\ if\ 75° < Z < 93°$ and $\mathrm{DHI} + \mathrm{BHI} > 50\,W/m^2$ $N/A\ if\ \mathrm{DHI} + \mathrm{BHI} < 50\,W/m^2$
	Diffuse fraction comparison	
k_d	N/A	$1.05\ if\ Z \leq 75°$ and $\mathrm{DHI} + \mathrm{BHI} > 50\,W/m^2$ $1.10\ if\ 75° < \mathrm{Z} < 93°$ and $\mathrm{DHI} + \mathrm{BHI} > 50\,W/m^2$ $N/A\ if\ \mathrm{DHI} + \mathrm{BHI} < 50\,W/m^2$

2.5. Statistical indicators

Several studies suggested performance indicators that can be used in radiation models for validations purposes [19,20]. Among those, three statistical indicators were chosen: normalized root mean squared error, normalized mean biased error, and the coefficient of determination. The nMBE consists of the

normalized average of the errors of a sample space thus allowing comparative analyses among different models. Positive values mean that the numerical model tends to under-predict the measured parameter, negative values indicate an over-estimation. It is worth highlighting that the use of nMBE alone is not recommended since this index can be subject to cancellation errors.

The nRMSE measures the variability of the errors between observed and simulated values. The nRMSE is not subject to cancellation errors; thus, the AHSRAE Guidelines [21] couples it with the nMBE index to verify the models' accuracy.

The R^2 index provides information on how close the simulated values are to the regression line of the observed values. It ranges from 0 to 1, where 0 indicates a complete mismatch between observed and simulated values and 1 a perfect match.

3. Results

3.1. Data quality check

The quality check of solar irradiation data recorded by the sun tracker in October 2021 and August 2022 is performed by assigning a QF to each observation. Figure 2 presents an overview of these quality flags.

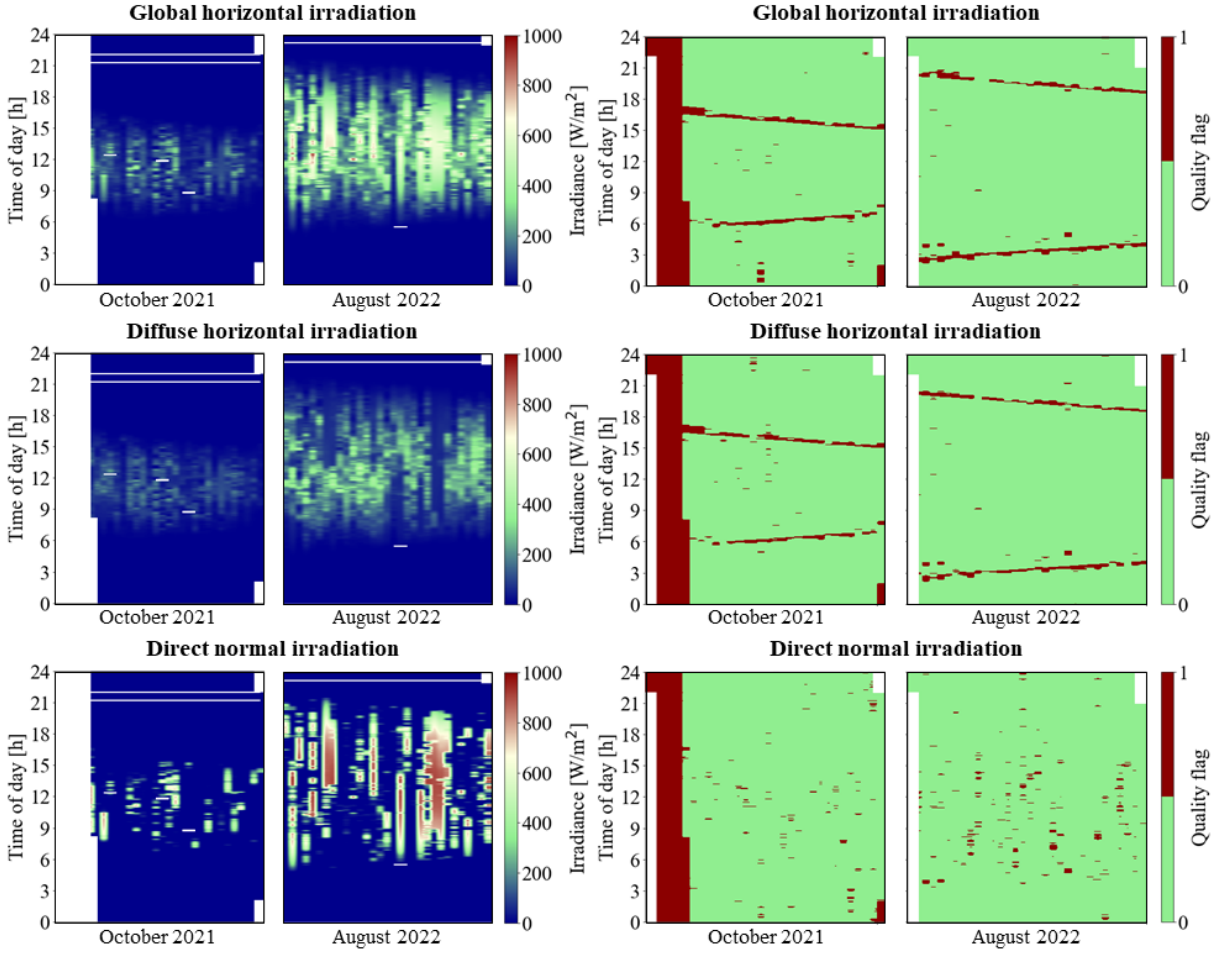

Figure 2. Overview of the solar irradiation data recorded in October 2021 and August 2022 by the sun tracker in Trondheim (left), and the corresponding quality flags (right).

A visual inspection of the diagrams suggests that erroneous measurements are mostly associated to low solar irradiation amounts (i.e., sunrise, sunset) and to particularly high values of DHI.

After the classification and filtering process, the datapoints that are suitable to be used in this validation study are reduced from 38,091 to 36,052 for October 2021 (ca. 9.5% discarded), and from 44,519 to 41,594 for August 2022 (ca. 9.3% discarded). Among these, only 14,378 datapoints in October 2021 and 27,940 datapoints in August 2022 are during daylight.

3.2. Decomposition modelling

3.2.1. October 2021. The results from the solar analysis performed in October 2021 are reported in Figure 3. On the one hand, the Yang4 model provides the most accurate estimation of the k_d (nMBE = 0.65%, nRMSE = 22.29%, R^2 = 0.97). The other three decomposition models (i.e., Skartveit3, Starke3, and Engerer4) show similar values of nMBE, nRMSE, and R^2 calculated for October 2021. Therefore, there is not a decomposition model which univocally performs worse than the others.

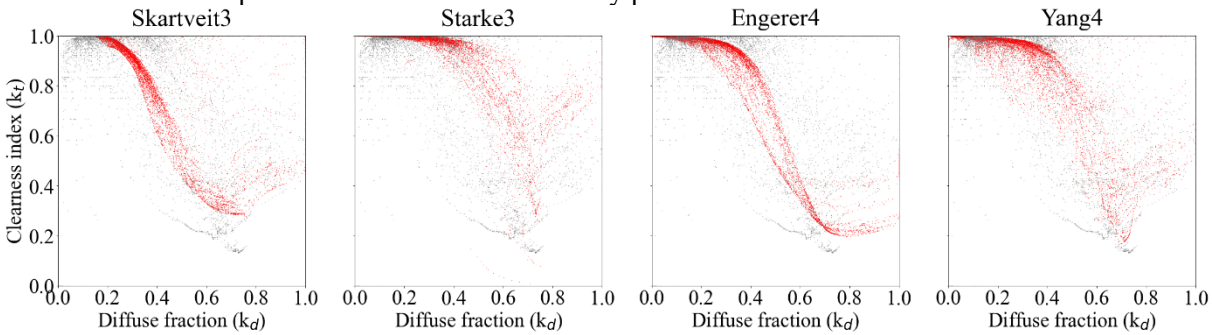

Figure 3. Observed k_t-k_d relationship (grey dots) and modelled k_t-k_d relationship (red dots), during October 2021.

3.2.2. August 2022. The results from the four decomposition models are reported in Figure 4. Yang4 model (nMBE=-0.54, nRMSE=17.18, R^2=0.96) is the most accurate together with the Engerer4 (nMBE=2.38, nRMSE=21.99, R^2=0.94) and the Skartveit3 (nMBE=1.97, nRMSE=20.58, R^2=0.95). The worst performance indicators are calculated for the Starke3 (Dfc) (nMBE=-11.91, nRMSE=30.42, R^2=0.88).

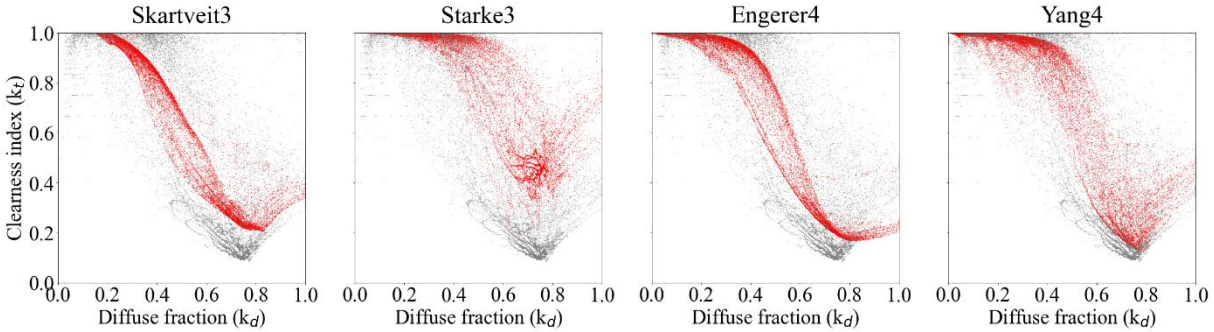

Figure 4. Observed k_t-k_d relationship (grey dots) and modelled k_t-k_d relationship (red dots), during August 2022.

4. Recommendation for solar decomposition at high latitudes

The outcomes from the experimental validation carried out in this study confirmed that the Yang4 model is the most accurate when applied at high latitudes (Table 2). Particularly during clear sky days (i.e., August 2022), the model was found to perform better than the other climate-specific and quasi-universal models. The lowest values of nMBE and nRMSE are always associated to the Yang4 model during both October 2021 (nMBE=0.65% and nRMSE=22.29%) and August 2022 (nMBE=-0.54% and nRMSE=17.18%). Similarly, the highest R^2 values are estimated for the Yang4 model (R^2=0.97 in October 2021 and R^2=0.97 in August 2022).

When it comes to climate-specific model (i.e., Starke3 model) and model parametrized with data from Norway (i.e., Skartveit3 model), the Skartveit3 model shows performance close to Yang4 model and outperformed both the Engerer4 and Starke3 models. In fact, the nMBE, nRMSE, and R^2 indicators are equal to 3.21%, 25.63%, and 0.96 in October 2021, and 1.97%, 20.58%, and 0.95 in August 2022, respectively.

In conclusion, the use of Yang4 model is recommended for applications at high latitudes being the most reliable decomposition model. However, the Skartveit3 model can also be exploited with similar results in terms of accuracy when all the information regarding the predictors of the Yang4 model (e.g., GHI, GHI_{extra}, GHI_{csky}, AST, Z, $k_{d,hourly}$ estimated with the Engerer2 model) are not available. In fact, the Skartveit3 model requires only the k_t and the Z as predictors. The results do not permit to extend these recommendations to other case study locations at higher latitudes such as Alta (Lat 69°58' N) and Longyearbyen (Lat 78°13′ N). This should be investigated numerically by exploiting the workflow described in this research study in other locations. In this regard, considering one case study location is the main limitation of the study.

Table 2. Statistical indicators calculated for the Skartveit3, Starke3, Engerer4, and Yang4 models, during October 2021 and August 2022.

	October 2021			**August 2022**		
	nMBE [%]	**nRMSE [%]**	**R^2**	**nMBE [%]**	**nRMSE [%]**	**R^2**
Skartveit3	3.21	25.63	0.96	1.97	20.58	0.95
Starke3	-3.56	28.46	0.95	-11.91	30.42	0.88
Engerer4	4.06	29.63	0.95	2.38	21.99	0.94
Yang4	0.65	22.29	0.97	-0.54	17.18	0.96

5. Final remarks and future developments

A local validation study is performed to verify the findings from worldwide validation studies [5,15] and to identify the most reliable decomposition model among Skartveit3, Starke3 (Dfc), Engerer4, and Yang4. The decomposition models are experimentally validated against solar irradiance data collected during October 2021 and August 2022, in Trondheim (Lat. 63° 26' 48.5772" N, Norway). Yang4 model, which was demonstrated to be the most reliable quasi-universal model, is confirmed to be the best also for Trondheim climate. However, the Skartveit3 couples a level of performance close to Yang4 with the low number of predictors required as input parameters.

Future developments of this study include: (i) the reiteration of the validation considering a longer time-frame (i.e., at least one year), (ii) the application of the same workflow to other case study locations and (iii) the validation of other decomposition models at high latitudes.

Acknowledgements

Authors acknowledge the financial support from the Research Council of Norway and various partners through the research projects “Enhancing Optimal Exploitation of Solar Energy in Nordic Cities through the Digitalization of the Built Environment” (Helios, project no. 324243).

References

[1] Statista 2022 Solar energy capacity in Norway from 2010 to 2021
[2] Formolli M, Lobaccaro G and Kanters J 2021 Solar energy in the Nordic built environment: challenges, opportunities and barriers *Energies* **14**
[3] Good C S, Lobaccaro G and Hårklau S 2014 Optimization of solar energy potential for buildings in urban areas - A Norwegian case study *Energy Procedia* vol 58 (Elsevier) pp 166–71
[4] Babar B, Luppino L T, Boström T and Anfinsen S N 2020 Random forest regression for improved mapping of solar irradiance at high latitudes *Sol. Energy* **198** 81–92

[5] Gueymard C A and Ruiz-Arias J A 2016 *Extensive worldwide validation and climate sensitivity analysis of direct irradiance predictions from 1-min global irradiance* vol 128 (Pergamon)
[6] Li Z, Xing H, Zeng S, Zhao J and Wang T 2017 Comparison of Anisotropic Diffuse Sky Radiance Models for Irradiance Estimation on Building Facades *Procedia Eng.* **205** 779–86
[7] Starke A R, Lemos L F L, Barni C M, Machado R D, Cardemil J M, Boland J and Colle S 2021 Assessing one-minute diffuse fraction models based on worldwide climate features *Renew. Energy* **177** 700–14
[8] Brito M C, Gomes N, Santos T and Tenedório J A 2012 Photovoltaic potential in a Lisbon suburb using LiDAR data *Sol. Energy* **86** 283–8
[9] Desthieux G, Carneiro C, Susini A, Abdennadher N, Boulmier A, Dubois A, Camponovo R, Beni D, Bach M, Leverington P and Morello E 2018 Solar Cadaster of Geneva: A Decision Support System for Sustainable Energy Management BT - From Science to Society ed B Otjacques, P Hitzelberger, S Naumann and V Wohlgemuth (Cham: Springer International Publishing) pp 129–37
[10] Brito M C 2020 Assessing the Impact of Photovoltaics on Rooftops and Facades in the Urban Micro-Climate *Energies* **13** 2717
[11] Desthieux G, Carneiro C, Camponovo R, Ineichen P, Morello E, Boulmier A, Abdennadher N, Dervey S and Ellert C 2018 Solar Energy Potential Assessment on Rooftops and Facades in Large Built Environments Based on LiDAR Data, Image Processing, and Cloud Computing. Methodological Background, Application, and Validation in Geneva (Solar Cadaster) *Front. Built Environ.* **4**
[12] Skartveit A, Olseth J A and Tuft M E 1998 An hourly diffuse fraction model with correction for variability and surface albedo *Sol. Energy* **63** 173–83
[13] Bright J M and Engerer N A 2019 Engerer2: Global re-parameterisation, update, and validation of an irradiance separation model at different temporal resolutions *J. Renew. Sustain. Energy* **11** 33701
[14] Engerer N A 2015 Minute resolution estimates of the diffuse fraction of global irradiance for southeastern Australia *Sol. Energy* **116** 215–37
[15] Yang D 2022 Estimating 1-min beam and diffuse irradiance from the global irradiance: A review and an extensive worldwide comparison of latest separation models at 126 stations *Renew. Sustain. Energy Rev.* **159** 112195
[16] Yang D and Boland J 2019 Satellite-augmented diffuse solar radiation separation models *J. Renew. Sustain. Energy* **11** 23705
[17] Yang D, Yagli G M and Quan H 2018 Quality Control for Solar Irradiance Data *2018 IEEE Innovative Smart Grid Technologies - Asia (ISGT Asia)* pp 208–13
[18] Long C N and Shi Y 2008 An Automated Quality Assessment and Control Algorithm for Surface Radiation Measurements *Open Atmos. Sci. J.* **2** 23–37
[19] Gueymard C A 2014 A review of validation methodologies and statistical performance indicators for modeled solar radiation data: Towards a better bankability of solar projects *Renew. Sustain. Energy Rev.* **39** 1024–34
[20] Taylor K E 2001 Summarizing multiple aspects of model performance in a single diagram *J. Geophys. Res. Atmos.* **106** 7183–92
[21] ASHRAE 2002 *Guideline 14-2002, measurement of energy and demand savings*